ADVANCED MATERIALS INTERFACES
Open Access
www.advmatinterfaces.de

A Supramolecular Wire Able to Self-Assemble on Gold Surface: Controlling the Film Length to Optimize the Device Lifetime and Electron Transfer Efficiency

Sascha Kubitzky, Raffaella Lettieri, Elena Passaretti, Mariano Venanzi, Marta De Zotti, Claudia Mazzuca, Ernesto Placidi, and Emanuela Gatto**

A chemical "lego nanoset" has been used to realize different structures on gold surfaces. Three building blocks have been designed, in order to chemically link the surface and self-assemble in an ordered manner. Self-assembled films are arranged on a gold surface into 3D suprastructures via consecutive deposition of different mono-layers, taken together by thymine-adenine hydrogen bonds. Three films, composed of one, two, and three helical peptide layers, both containing a zinc-tetraphenylporphyrin dye as an external sheet, are built and characterized by spectro-electrochemical and spectroscopic techniques. All films are found to generate current under illumination, and their photoresponse and stability are studied as a function of the number of peptide layers. The efficiency of the photoconversion process has been correlated to the molecular organization of the porphyrin dyes in the film and to the templating role of the bridge between the porphyrin and the gold surface.

1. Introduction

The creation of supramolecular materials on the surface, in which the constituent units are highly regular molecular nanostructures, is one of the great challenges for materials science.[1,2] The self-assembly of oligomers into supramolecular polymers, held together with directional and reversible secondary interactions, has the potential for generating such nanostructures.[3] Learning how to create large supramolecular units, and the elucidation of rules mediating their macroscopic organization into functional properties, will offer a fascinating prospect for technology and open up the prospect of many new applications.[4]

One of such challenging application is artificial photosynthesis, as the perfect positioning of different redox centers into supramolecular wires may be of fundamental importance in controlling the direction of electronic flow.[5–7] Another significant application is photodynamic therapy, in which nanostructures able to promote the formation of singlet oxygen are used to kill tumor cells. The efficiency of the electron transfer process can be regulated by controlling the film length and in particular the distance of the electron transfer donor from the electrode surface.[8] Specifically, in a non-adiabatic regime, the electron transfer (ET) rate from the gold electrode to the redox species (or vice versa) decreases by increasing the distance.[9–11] In general, the effect of the distance of the redox species from the surface influences the ET efficiency, also because the gold electrode may quench the dye-excited singlet state via energy transfer. This process depends on the distance, and, for this reason, radiative processes are less efficient by reducing the distance from the surface. However, a short distance of the dye from the surface favors higher efficiencies since the superexchange rate constant decreases with the increase in chain length.

Also in peptide systems, the effect of the distance on the rate constant depends on the peptide length and secondary structure.[12–15] In a system shorter than 20 Å, the prevalent ET mechanism is superexchange, which is characterized by an exponential decrease of the electron transfer rate constant with the distance, depending on the tunneling factor β. In longer systems, the hopping mechanism is prevalent, in which the electron transfer rate constant is inversely proportional to the distance.[12,15]

S. Kubitzky, R. Lettieri, M. Venanzi, C. Mazzuca, E. Gatto
Department of Chemical Science and Technologies
University of Rome Tor Vergata
Rome 00133, Italy
E-mail: emanuela.gatto@uniroma2.it

S. Kubitzky
Department of Chemistry
Biology and Biotechnology
University of Perugia
Perugia 06123, Italy

E. Passaretti
Institute for Building Materials
Eidgenössische Technische Hochschule
Zürich 8093, Switzerland

M. De Zotti
Department of Chemical Sciences
University of Padova
Padova 35131, Italy
E-mail: marta.dezotti@unipd.it

E. Placidi
Department of Physics
Sapienza University of Rome
Rome 00185, Italy

The ORCID identification number(s) for the author(s) of this article can be found under https://doi.org/10.1002/admi.202400418

DOI: 10.1002/admi.202400418

Furthermore, the bridge between the donor–acceptor pair influences the rate of the process. In particular, the tunneling parameter found in helical peptides may reach the value of 0.02 $Å^{-1}$.[16,17] As matter of fact, photosynthetic proteins have mostly helical conformations, but this kind of secondary structure can be obtained only in long peptides, due to thermodynamic reasons. Short peptides populate in general disordered conformations. In order to optimize the distance between the redox species and the surface, still maintaining the helical conformation, our research group has developed many α-aminoisobutyric acid (Aib) -based peptides, that are helical even if composed of a very short number of residues.[18–21] Aib is a C_α-tetrasubstituted amino acid, that imposes a marked restriction on the available ϕ, Ψ space, constraining short peptides to populate helical conformations.[22,23]

In the literature, many 2D systems of different length have been studied, in order to investigate the effect of the peptide bridge length on the ET efficiency.[24–30] To our knowledge, no studies concerning ET efficiency of different multilayers has been reported in the literature, and in particular, the effect of the film length on the photoinduced electron transfer performances has never been studied in this kind of systems.

In a previous publication, we showed the excellent performances of 3D supramolecular peptide systems on gold surfaces, realized by exploiting thymine-adenine interaction.[31] Specifically, we have studied and compared the excellent ET properties of two supramolecular systems: Film **1** composed of adenine linked to lipoic acid (Lipo-A) covalently bound to the gold surface, and a zinc-tetraphenylporphyrin chromophore (ZnTPP) linked to a thymine (T-ZnTPP). 5 Film **2** had an additional noncovalently linked layer: a helical undecapeptide analog of the natural peptide trichogin GA IV,[32] in which four glycines were replaced by as many lysines to impart water solubility and reduce flexibility.[32,33] The presence of Lys residues also confers pH sensitivity to the peptide secondary structure.[32,34] The peptide termini were functionalized with thymine and adenine, respectively, to enable Lipo-A and T-ZnTPP conjugation. Interestingly, using this system, we also demonstrated that α-helix is more efficient than 3_{10} helix in the photoinduced electron transfer process.[34]

In this work, we want to demonstrate that with similar systems, by exploiting the thymine-adenine interaction, we can build multilayer supramolecular films, in which we are able to control the film length and the number of layers, and thus the electron transfer and photocurrent efficiency. To this aim, we have assembled one, two, or three layers of a dipeptide composed of two Aib residues, functionalized at the peptide termini with thymine and adenine (T-Aib-Aib-A). Aib residues favor helical conformation even with very short peptides. Film **4** consisted of adenine linked to lipoic acid (Lipo-A) covalently bound to the gold surface, an additional noncovalently linked layer composed of T-Aib-Aib-A and a zinc-tetraphenylporphyrin chromophore (ZnTPP) linked to a thymine (T-ZnTPP). Film **5** and **6** were composed, respectively, of two and three layers of this peptide film (**Figure 1**).

2. Results and Discussion

Experimental details on the synthesis of molecular components and the film depositions are reported elsewhere.[35,36] Similar systems in solution could form long filaments through complementary nucleobase interaction by properly tuning the experimental conditions.[32,35,36] We avoided the formation of peptide filaments on the surface, by using a diluted peptide solution (10 µm, e.g., 10 times below the threshold to get the self-assembly, see the Supporting Information) for details, thus obtaining a monolayer.[31]

The films were deposited on a gold (5 nm)-coated glass slide to perform absorption and fluorescence spectroscopy measurements. The absorption spectra reported in **Figure 2** not only confirmed the presence of the film on the surface but also could be used to determine the amount of porphyrin molecules from the measured absorbance value.[31,37] This value was $(0.9 \pm 0.8) \times 10^{-10}$ mol cm^{-2} for film **4** (one peptide layer), and $(1.5 \pm 0.4) \times 10^{-10}$ mol cm^{-2} for film **5** (two peptide layers) and $(1.0 \pm 0.5) \times 10^{-10}$ mol cm^{-2} for film **6** (three peptide layers). These values suggest the presence of a high density of porphyrins on surface, taking into account their mean molecular area. However, the mean molecular area occupied by the T–ZnTPP layer in the three films is 183 $Å^2$ for film **4**, 107 $Å^2$ for film **5** and 166 $Å^2$ for film **6**, suggesting in all of them, a close packing of the porphyrin ring, that is supposed to stand up on the gold surface[38,39] (the calculated size[40] of the T–ZnTPP molecule is 402 $Å^2$ in a planar arrangement and 100 $Å^2$ in a vertical arrangement).

This result is supported by the surface absorption spectra, which show a bathochromic shift of the Soret band, suggesting the presence of J-aggregates in films **4**, **5**, and **6** (Figure 2 and **Table 1**). Interestingly, the shift observed in film **4** (absorption maximum at 429.9 nm) is higher than the one observed in film **6** (absorption maximum at 428.4 nm) that is higher than the one observed in film **5** (absorption maximum at 428.1 nm), indicating that the highest quantity of J aggregates should be present in film **4**, despite the lower intensity of the absorption maximum.

The fluorescence emission spectra exhibit the typical emission band of the ZnTPP fluorophore, with two maxima at 607 and 660 nm, which confirms the T-ZnTPP inclusion into the films (**Figure 3**). The fluorescence spectra on Au/glass surface are broader compared to those obtained in solution, and slightly redshifted, suggesting aggregation among the porphyrins in all the films. Interestingly, the F/A value, which is proportional to the quantum yield, increases by increasing the number of the peptide layers, which is with the film length (Figure 3).

It is well known that the gold electrode quenches the porphyrin-excited singlet state via energy transfer. This process is distance-dependent and if the multi-peptide T-$(Aib)_2$-A layer is formed, should be more efficient with film **4**, in which the ZnTPP is closer to the gold surface, giving rise to a lower fluorescence intensity, than with film **5** and lastly with film **6**, in which the ZnTPP is farther away from the gold surface.

Figure 3 confirms our hypothesis of the multilayer formation since the intensity of the spectra normalized by the absorption is: film **6**>film**5**>film**4**, which follows, respectively, the trend expected for three, two and one peptide layer formation.

FTIR-RAS measurements have been performed to determine the presence of the peptide moiety in the film and its orientation (Figure S2, Supporting Information). FTIR spectra of all three films without the porphyrin moiety, show in the 1750–1450 cm^{-1} region, bands at ≈1730, 1680, and 1490 cm^{-1} that are assignable to thymine[41] and bands at 1680, 1610, and 1580 cm^{-1} which are attributable to adenine.[42] Finally broad bands at ≈1635 and 1540 $cm^{-1}$are Amide I and Amide II bands due to peptides,[43,44]

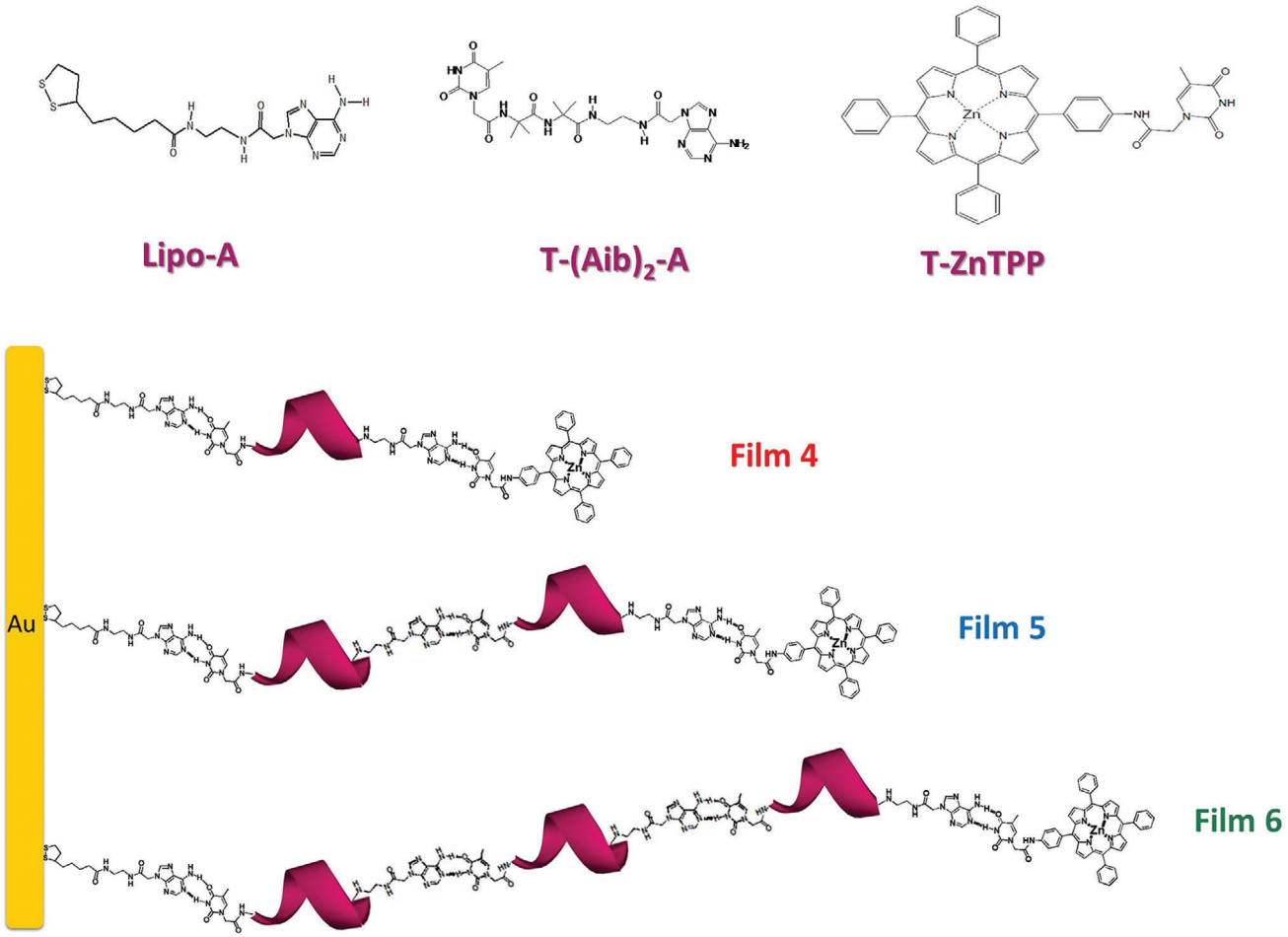

Figure 1. Chemical structures of the building blocks used for the construction of films **4**, **5,** and **6**.

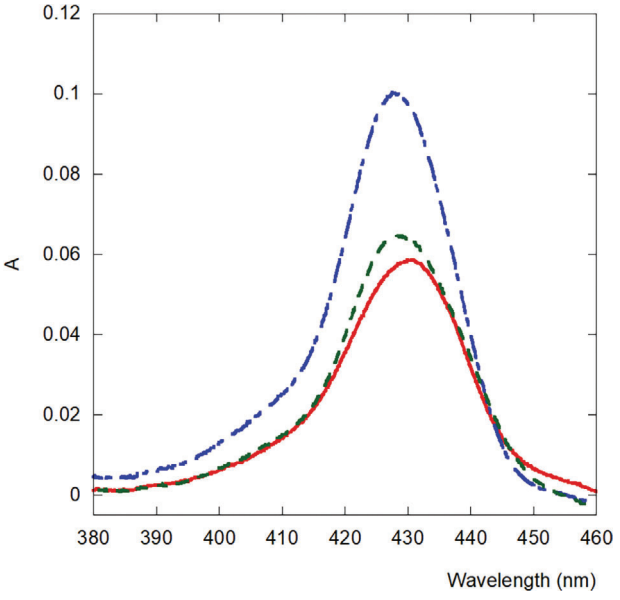

Figure 2. UV–vis spectra of film **4** (red), **5** (blue), and **6** (green) on Au/glass surfaces in transmission mode.

demonstrating the presence of the peptide in all the three films. However, due to the low number of amino acids constituting the peptide moiety, it is very difficult to define a well-defined secondary structure and consequently, the molecular orientation with respect to the gold surface.

In order to characterize the surface morphology atomic force measurements have been performed on the three films. AFM measurements showed the presence of some structures of variable sizes (ranging from a few to a few tens of nanometers) (**Figure** 4a–c). The average height of these structures is ≈13 nm. However, cyclic voltammetry experiments show that the electrode is fully passivated by the supramolecular systems investigated (Figure S3, Supporting Information), that together with the high T-ZnTPP surface coverage values obtained, demonstrate that the films are homogeneous. Probably the structures with different height correspond to areas where there is a multilayer of the peptide system on the surface, in which the thickness of the film is higher.

In a previous paper, we have used similar films for their capability to give rise to oxygen photoreduction. Herein, we performed photocurrent generation measurements in the ZnTPP absorption range in order to study the effect of the peptide length on the electron transfer efficiency.

Table 1. Results obtained using UV–vis absorption and fluorescence emission spectroscopy, in transmission mode (directly on surface).

Film	Molecular density [mol cm^{-2}]	Mean molecular area [Å^2]	Absorbance maximum	Maximum wavelength absorption [nm]	Maximum wavelength emission [nm]	Emission maximum intensity [F/A] · 10^5
Film 4	0.9×10^{-10}	183	0.058	429.9	606	2.9
					657	6.0
Film 5	1.5×10^{-10}	107	0.100	428.1	607	3.1
					658	6.7
Film 6	1.0×10^{-10}	166	0.064	428.4	608	3.7
					661	8.5

Upon illumination in the visible region and in the presence of a supporting electrolyte (sodium sulphate, Na_2SO_4), high cathodic currents were generated.[31,34] The electron acceptor in the present system was demonstrated to be O_2 in solution.[31,34] Photocurrent responses of films **4**, **5** and **6** are shown in **Figure 5**. The photocurrent action spectrum is very similar to the surface absorption spectrum of ZnTPP, confirming that ZnTPP is the photoexcited species responsible for the signal.

Interestingly, a significant enhancement in the magnitude of the photocurrent upon inserting the peptide between Lipo–A and the deposited T–ZnTPP SAM was observed, with all three films having a higher photocurrent value than film **1** (without the peptide). Furthermore, the value obtained with film **5** is higher than the one obtained with films **4** and **6** (Figure 5). However, the photocurrent value is not indicative of the efficiency of the process, since the higher the absorption value, the higher is the number of molecules able to give rise to photo-induced current. For this reason, we have calculated and compared the photocurrent quantum yield values, since they are normalized for this parameter (Supporting Information). Still, also the quantum efficiencies obtained with the three films (**Table 2**) demonstrated that all three films are more efficient (ϕ = 0.34–0.49%) than film **1** (without the peptide, ϕ = 0.3%) and that films **5** and **6** are the best in performing this kind of measurements (ϕ = 0.49%). These values are higher than those reported for ZnTPP systems on both indium tin oxide (ITO)[45,46] and gold.[31,47] When a negative potential was applied, the efficiency increased, reaching 0.7% for film **4**, 0.9% for film **5** and 1.0% for film **6** at an applied potential of −0.2 V. These values are higher than those obtained with other porphyrin–peptide systems covalently linked to a gold surface,[45,46] but are lower than a similar system previously reported by us.[31]

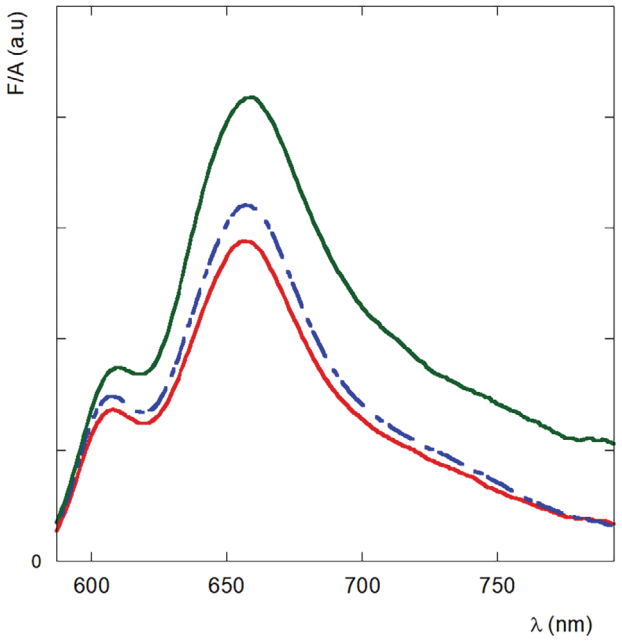

Figure 3. Fluorescence spectra of film **4** (red), **5** (blue), and **6** (green) on Au/glass substrate; λex = 433 nm. The spectra are normalized for the absorption value at the excitation wavelength.

Electron transfer in peptides depends on the distance and a mechanism transition from tunneling to hopping is obtained at a distance ≈20 Å.[15] In those systems, the peptide length is quite short (two Aib residues in helical conformation correspond to a distance of 4 Å). From crystallography the length of the complete A-(Aib)$_2$-T molecules is 15 Å.[35] However, film **4** is more performing than the reference film **1**, suggesting that also the presence of only two residue peptides in a helical conformation can influence the photoinduced electron transfer efficiency. In particular, all the films containing the peptides have a higher photocurrent yield compared to the reference film **1** (**Figure 6**).

The reason for the higher photocurrent value obtained with film **5** and **6** might be multi-fold.

First, as already reported, the gold electrode quenches the porphyrin-excited singlet state via energy transfer. This process depends on distance, for this reason this effect should be more efficient with film **4**, in which the ZnTPP is closer to the gold surface, giving rise to a lower photocurrent value, less in film **5** and very low in film **6**.

Second, the ET rate from the gold electrode to the resulting porphyrin cation radical decreases with an increase in the chain length, favoring a higher photocurrent value in film **4**, then in film **5**, and lastly in film **6**. Third, the presence of porphyrin aggregation enhances the rate of the nonradiative pathway in the excited state, so in general, a decrease in the efficiency. Most likely film **5** is the one in which the combination of the gold quenching and distance-dependence ET are optimized.

However, fluorescence microscopy images show that film **5** is the one in which the porphyrin domain formation is enhanced, giving rise to a higher surface density (**Figure 7**). It has already been demonstrated that porphyrin aggregation and molecular orientation influence photocurrent efficiency.[45–47] As a matter of fact, in the film **2** previously reported,[31] in which between

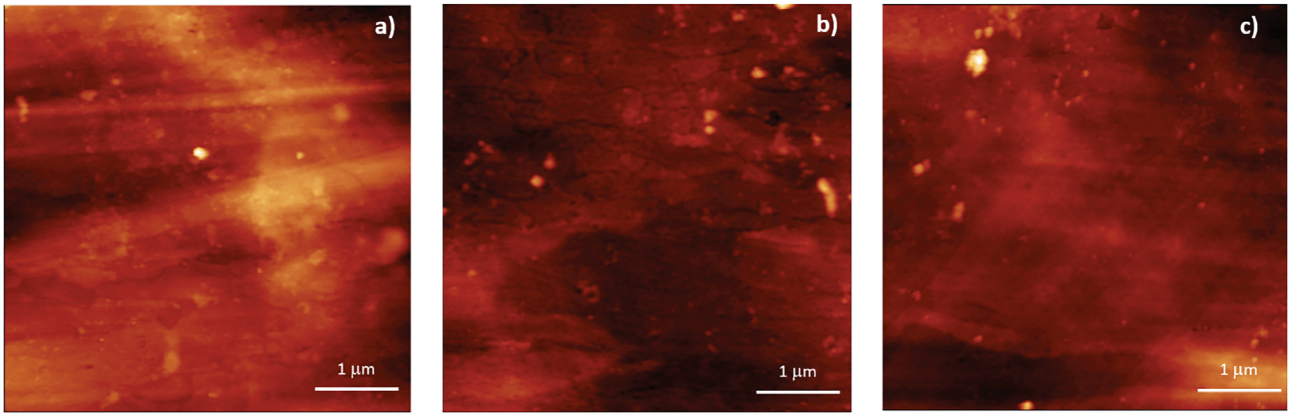

Figure 4. AFM image of the gold surface after the film **4** (a), film **5** (b) and film **6** (c) deposition.

the Lipo-A and the T-ZnTPP is an undecapeptide analog of the Thricogin GA IV peptide, denoted as film **2**, the distance of the porphyrin from the surface (63 Å in 3_{10} helical conformation), is very similar to that of film **5** (62 Å), but the photocurrent efficiency is higher. This means that for the same distance from the gold, a film composed of a single and longer peptide is more efficient than a film composed of multilayers of short peptides and nucleobases, confirming again that helical peptides are a better ET templating medium than a mix of nucleobases and short peptides.

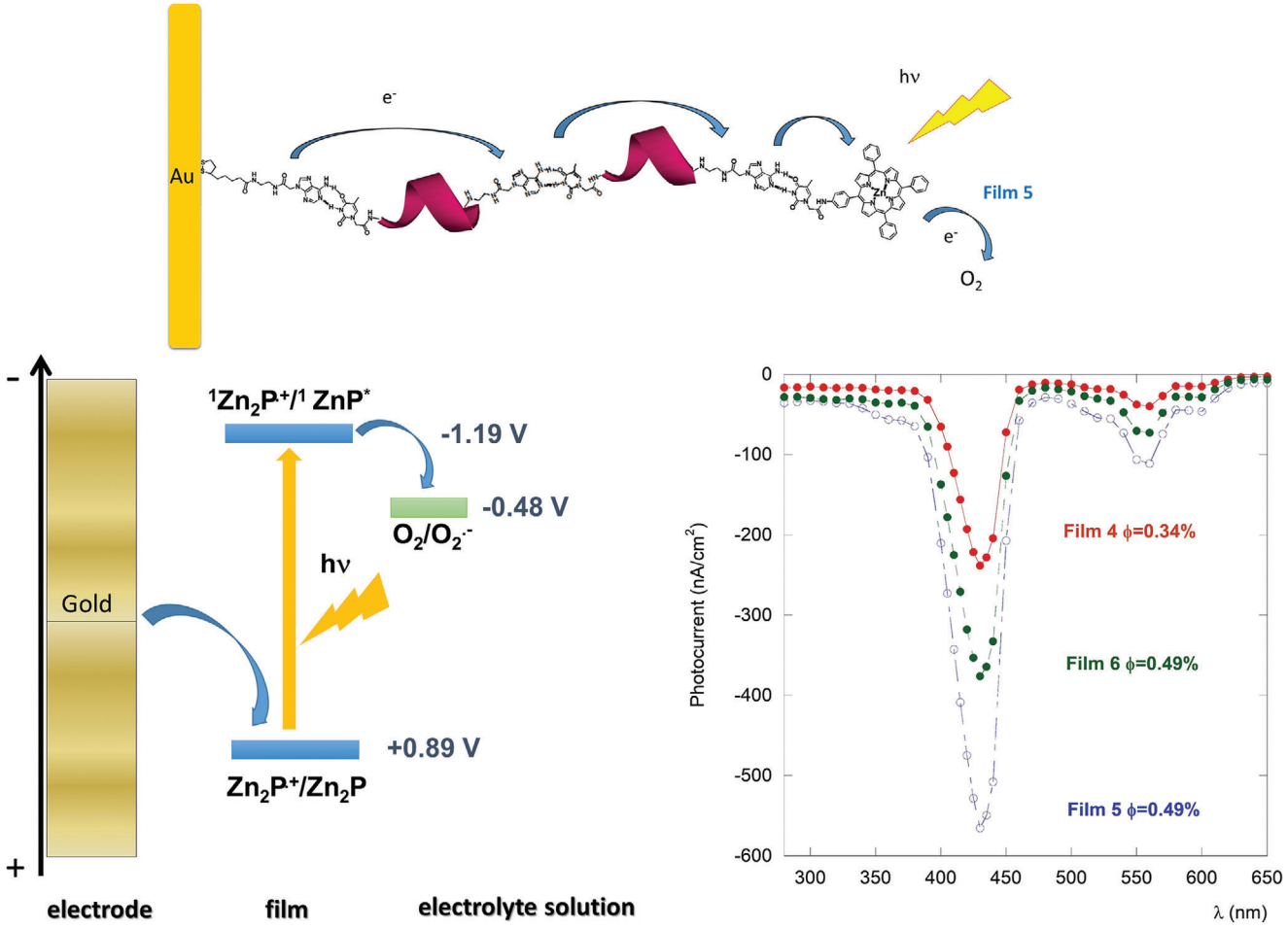

Figure 5. a) Scheme of the electron flow in film 5; b) photocurrent generation diagram indicating the path of the electron flow; c) photocurrent action spectra of film **4** (red), **5** (blue), and **6** (green).

Table 2. Results obtained using photoelectrochemical measurements.

Film	Absorbance at the maximum	Maximum photocurrent value at 430 nm	Quantum efficiency ϕ	Photocurrent value at 430 nm after two weeks
Film 4	0.058	−238 nA cm^{-2}	0.34%	−85 nA cm^{-2}
Film 5	0.100	−565 nA cm^{-2}	0.49%	−308 nA cm^{-2}
Film 6	0.064	−376 nA cm^{-2}	0.49%	−374 nA cm^{-2}

The reasons for that are related to the different mechanisms of ET and to the templating properties of the two systems (helical peptides and nucleobases). It is well known that electrons can migrate through DNA in a multistep hopping process, in which the nucleotide bases act as stepping stones.[48–50] Short peptides, instead, exploit a superexchange mechanism, which allows faster ET rate constants, promoting direct ET from the Au electrode to ZnTPP. In particular, in helical peptides the intramolecular hydrogen bonds actively promote ET, and also the dipole moment[51] and the spin may affect the ET.[52–54] Helical peptides, furthermore have the capability to self-organize on the surface in an ordered manner, creating an oriented 2D array, thus increasing the molecular density on the surface, assuring ET directionality and avoiding dyes aggregation,[20b] as demonstrated by spectroscopy measurements and fluorescence microscopy images, that show fewer peptide aggregates in film **2** compared to film **5** (**Figure 8**).

Not all the films were stable in time. In particular, film **4** showed a 64% photocurrent signal decrease after 2 weeks, film **5** showed a 45% photocurrent decrease, while film **6** was found to be stable, giving rise to the same photocurrent intensity for more than two months (stored at ambient temperature). These results indicate that the longer the film length, the higher the stability. However, since the length of film **2** is similar to that of film **5** which is unstable, again we demonstrate that a longer helical peptide gives rise to a more stable film compared to a multilayer film with the same length. These findings strongly suggest that for a long life device, elongated helical peptides are the best option, while for quickly biodegradable devices the best results are achieved using shorter helical peptide building blocks.

3. Conclusion

In summary, all these results clearly indicate that the bio-inspired non-covalent strategy developed in the present work is a potentially effective and simple means by which to engineer complex modular supramolecular SAMs to control film length, its stability over time and the process efficiency for device fabrication purposes, including the conversion of incident light to electronic current and oxygen photoreduction for photodynamic therapy.

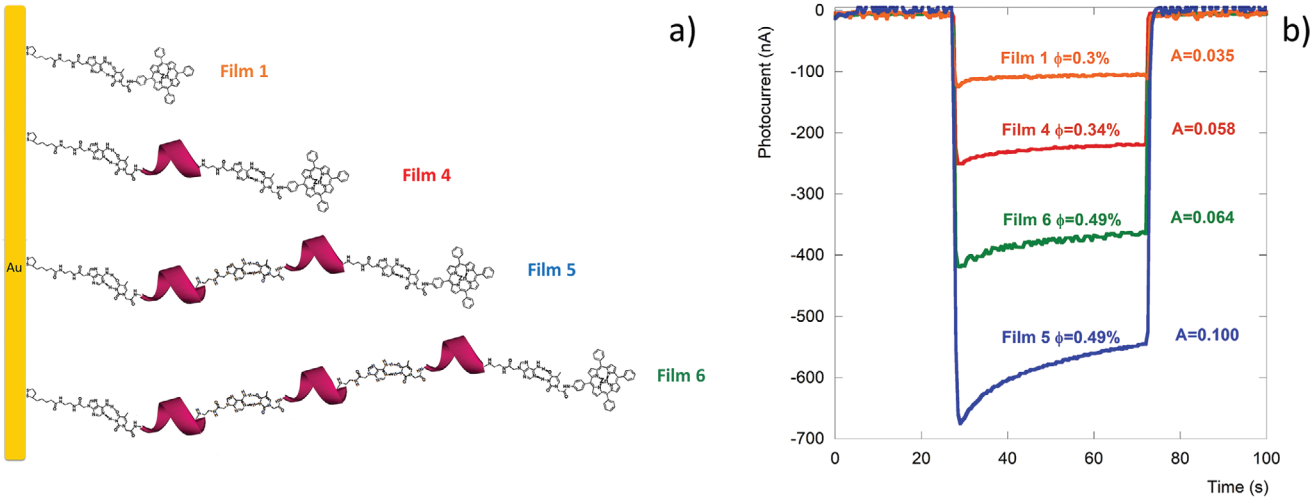

Figure 6. a) Scheme of the films on surface; b) photocurrent signal obtained by exciting film **1**, film **4**, film **5** and film **6** at 430 nm.

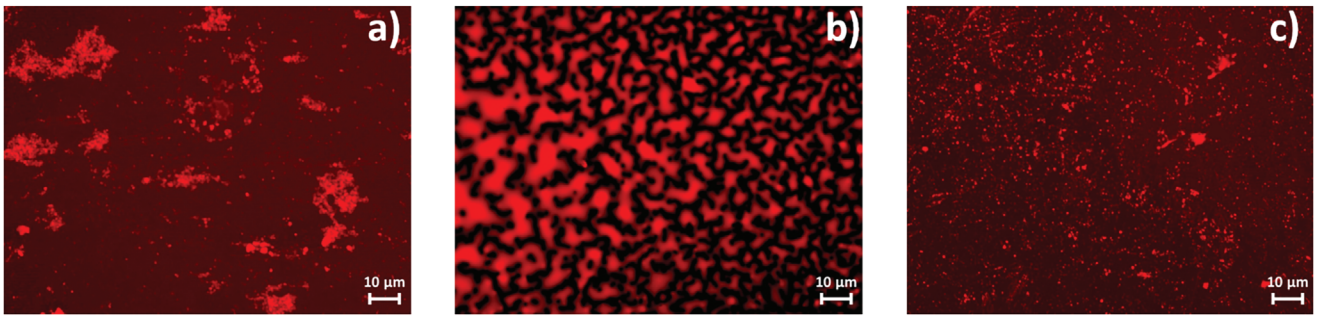

Figure 7. Fluorescence microscopy images of film **4** (a), **5** (b), and **6** (c) on Au/glass substrate.

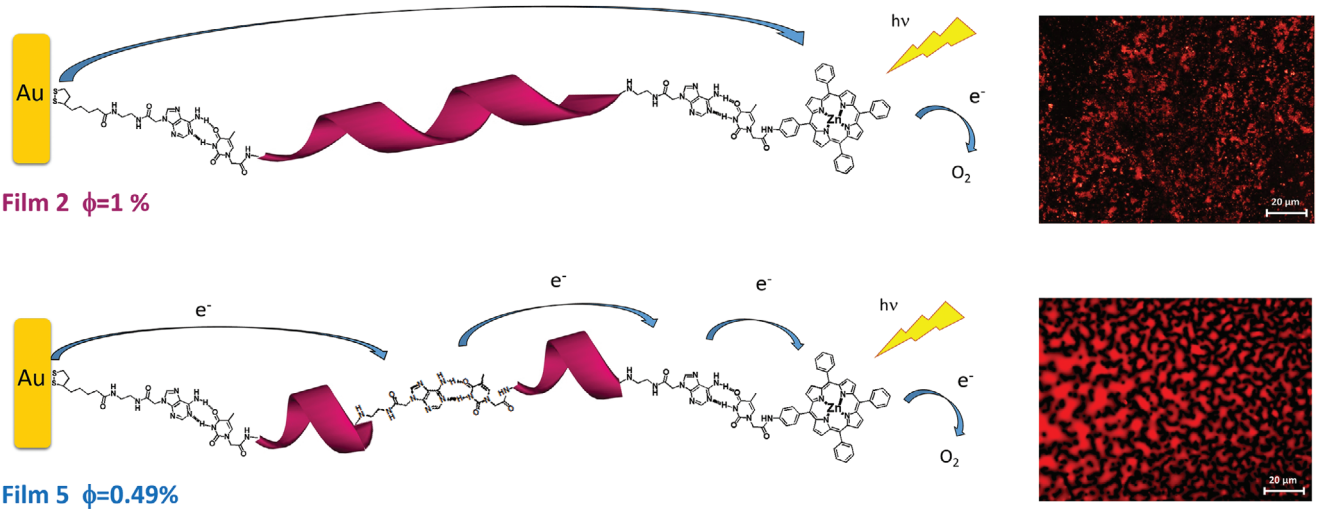

Figure 8. a) Photocurrent generation diagram indicating the path of the electron flow in film **2** and film **5**; fluorescence microscopy of film **2** (top) and film **5** (bottom) on Au/glass substrate.

Supporting Information

Supporting Information is available from the Wiley Online Library or from the author.

Acknowledgements

This work was supported by MUR (Rome, Italy) (PRIN2022, grant no. 2022EPWFER).

Conflict of Interest

The authors declare no conflict of interest.

Associated Content

Synthesis of the T-$(Aib)_2$-A building block and its NMR characterization, FTIR-RAS measurements, cyclic voltammetry measurements, experimental details.

Data Availability Statement

The data that support the findings of this study are available from the corresponding author upon reasonable request.

Keywords

peptides, photocurrent generation, self assembled monolayers, supramolecular chemistry, thymine-adenine interactions

Received: May 27, 2024
Revised: September 30, 2024
Published online:

[1] E. Mattia, S. Otto, *Nat. Nanotechnol.* **2015**, *10*, 111.
[2] J. Martin, M. Martin-Gonzalez, J. F. Fernandez, O. Caballero-Calero, *Nat. Commun.* **2014**, *5*, 5130.
[3] *Supramolecular Chemistry on Surfaces: 2D Networks and 2D Structures*, (Ed.: N. Champness), John Wiley & Sons, USA **2021**.
[4] C. Li, A. Iscen, H. Sai, K. Sato, N. A. C. Sather, S. M. Z. Alvarez, L. C. Palmer, G. C. Schatz, S. Stupp, *Nat. Mater.* **2020**, *19*, 900.
[5] (a) M. Morisue, S. Yamatsu, N. Haruta, Y. Kobuke, *Chem. - Eur. J.* **2005**, *11*, 5563. (b) D. M. Guldi, *Chem. Soc. Rev.* **2002**, *31*, 22. (c) W. Kim, E. Edri, H. Frei, *Acc. Chem. Res.* **2016**, *49*, 1634.
[6] M. E. El-Khouly, E. El-Mohsnawy, S. Fukuzumi, *J. Photochem. Photobiol. C: Photochem. Rev.* **2017**, *31*, 36.
[7] (a) V. Balzani, A. Credi, M. Venturi, *ChemSusChem.* **2008**, *1*, 26; (b) J. Barber, *Chem. Soc. Rev.* **2009**, *38*, 185.
[8] A. J. Bard, L. R. Faulkner, *Electrochemical Methods, Fundamentals and Applications*, John Wiley & Sons, USA **2001**.
[9] R. A. Marcus, N. Sutin, *Biochim. Biophys. Acta.* **1985**, *811*, 265.
[10] N. S. Hush, *Coord. Chem. Rev.* **1985**, *64*, 135.
[11] J. R. Bolton, M. Mataga, G. Mc. Lennon, *Introduction to Electron Transfer in Inorganic, Organic, and Biological Systems*, ACS Publication, Washington, DC, USA **1991**.
[12] E. Gatto, M. Caruso, M. Venanzi, *The Electrochemistry of Peptide Self-Assembled Monolayers*, (Eds.: M.Aliofkhazraei, A.Makhlouf), Springer, Berlin, Germany **2016**.
[13] Y. T. Long, E. Abu-Irhayem, H. B. Kraatz, *Chem. - Eur. J.* **2005**, *11*, 5186.
[14] M. Cordes, B. Giese, *Chem. Soc. Rev.* **2009**, *38*, 892.
[15] R. A. Malak, Z. Gao, J. F. Wishart, S. S. Isied, *J. Am. Chem. Soc.* **2004**, *126*, 13888.
[16] M. Kai, K. Takeda, T. Morita, S. Kimura, *J. Pept. Sci.* **2008**, *14*, 192.
[17] H. S. Mandal, H. B. Kraatz, *J. Phys. Chem. Lett.* **2012**, *3*, 709.
[18] E. Gatto, A. Porchetta, M. Scarselli, M. De Crescenzi, F. Formaggio, C. Toniolo, M. Venanzi, *Langmuir* **2012**, *28*, 2817.
[19] M. Caruso, P. Flamini, E. Gatto, E. Placidi, G. Ballano, F. Formaggio, C. Toniolo, D. Zanuy, C. Alemán, M. Venanzi, *Soft Matter.* **2014**, *10*, 2508.
[20] E. Gatto, A. Quatela, M. Caruso, R. Tagliaferro, M. De Zotti, F. Formaggio, C. Toniolo, A. Di Carlo, M. Venanzi, *ChemPhysChem.* **2014**, *15*, 64.
[21] M. Venanzi, E. Gatto, M. Caruso, A. Porchetta, F. Formaggio, C. Toniolo, *J. Phys. Chem. A* **2014**, *118*, 6674.
[22] C. Toniolo, M. Crisma, F. Formaggio, C. Peggion, *Biopolymers (Pept Sci)*. **2001**, *60*, 396.
[23] P. Balaram, *Curr. Opin. In Struct. Biol.* **1992**, *2*, 845.

[24] S. Sek, A. Tolak, A. Misicka, B. Palys, R. Bilewicz, *J. Phys.Chem. B* **2005**, *109*, 18433.
[25] J. Watanabe, T. Morita, S. Kimura, *J. Phys. Chem. B* **2005**, *109*, 14416.
[26] S. Sek, A. Sepiol, A. Tolak, A. Misicka, R. Bilewicz, *J. Phys. Chem. B* **2004**, *108*, 8102.
[27] Y. Arikuma, K. Takeda, T. Morita, M. Ohmae, S. Kimura, *J. Phys. Chem. B* **2009**, *113*, 6256.
[28] H. S. Mandal, H. B. Kraatz, *Chem. Phys.* **2006**, *326*, 246.
[29] Y. Arikuma, H. Nakayama, T. Morita, *Angew. Chem., Int. Ed.* **2010**, *49*, 1800.
[30] Y. Arikuma, H. Nakayama, T. Morita, S. Kimura, *Langmuir* **2011**, *27*, 1530.
[31] E. Gatto, S. Kubitzky, M. Schriever, S. Cesaroni, C. Mazzuca, M. Venanzi, M. De Zotti, *Angew. Chem., Int. Ed.* **2019**, *58*, 7308.
[32] M. De Zotti, B. Biondi, C. Peggion, F. Formaggio, Y. Park, K. S. Hahm, C. Toniolo, *Org. Biomol. Chem.* **2012**, *10*, 1285.
[33] C. Peggion, F. Formaggio, M. Crisma, R. F. Epand, R. M. Epand, C. Toniolo, *J. Pept. Sci.* **2003**, *9*, 679.
[34] S. Kubitzky, M. De Zotti, B. Biondi, M. Venanzi, E. Gatto, *Chem. Eur. J.* **2021**, *27*, 2810.
[35] G. Marafon, D. Mosconi, D. Mazzier, B. Biondi, M. De Zotti, A. Moretto, *RSC Adv.* **2016**, *6*, 73650.
[36] G. Marafon, I. Menegazzo, M. De Zotti, M. Crisma, C. Toniolo, A. Moretto, *Soft Matter* **2017**, *13*, 4231.
[37] F. Sabuzi, V. Armuzza, V. Conte, B. Floris, M. Venanzi, P. Galloni, E. Gatto, *J. Mater. Chem. C* **2016**, *4*, 622.
[38] H. Imahori, H. Norieda, Y. Nishimura, I. Yamazaki, K. Higuci, N. Kato, T. Motohiro, H. Yamada, K. Tamaki, M. Arimura, Y. Sakata, *J. Phys. Chem. B* **2000**, *104*, 1253.
[39] H. Imahori, T. Hasobe, H. Yamada, Y. Nishimura, I. Yamazaki, S. Fukuzumi, *Langmuir* **2001**, *17*, 4925.
[40] The molecular areas have been calculated using the UCSF Chimera software. E. F. Pettersen, T. D. Goddard, C. C. Huang, G. S. Couch, D. M. Greenblatt, E. C. Meng, T. E. Ferrin, *J. Comput. Chem* **2004**, *25*, 1605.
[41] M. Mohammed, A. M. Seuvre, J. L. Koenig, *Carbohydr. Res.* **1984**, *134*, 23.
[42] M. Mohammed, A. M. Seuvre, J. L. Koenig, *Carbohydr. Res.* **1984**, *131*, 1.
[43] M. Boncheva, H. Vogel, *Biophys. J* **1997**, *73*, 1056.
[44] Y. Miura, S. Kimura, Y. Imanishi, J. Umemura, *Langmuir* **1999**, *15*, 1155.
[45] H. Uji, K. Tanaka, S. Kimura, *J. Phys. Chem. C* **2016**, *120*, 3684.
[46] B. J. Walker, A. Dorn, V. Bulović, M. G. Bawendi, *Nano Lett.* **2011**, *11*, 2655.
[47] H. Uji, Y. Yatsunami, S. Kimura, *Phys. Chem. C* **2015**, *119*, 8054.
[48] A. Nano, A. L. Furst, M. G. Hill, J. K. Barton, *J. Am. Chem. Soc.* **2021**, *143*, 11631.
[49] B. Giese, *Curr. Op. Chem. Biol.* **2002**, *6*, 612.
[50] F. Boussicault, M. Robert, *Chem. Rev.* **2008**, *108*, 2622.
[51] S. Yasutomi, T. Morita, Y. Imanishi, S. Kimura, *Science* **2004**, *304*, 1944.
[52] A. C. Aragonès, E. Medina, M. Ferrer-Huerta, N. Gimeno, M. Teixidó, J. L. Palma, N. Tao, J. M. Ugalde, E. Giralt, I. Díez-Pérez, V. Mujica, *Small* **2017**, *13*, 1602519.
[53] M. Kettner, B. Göhler, H. Zacharias, D. Mishra, V. Kiran, R. Naaman, C. Fontanesi, D. H. Waldeck, S. Sek, J. Pawlowski, J. Juhaniewicz, *J. Phys. Chem. C* **2015**, *119*, 14542.
[54] F. Tassinari, D. R. Jayarathna, N. Kantor-Uriel, K. L. Davis, V. Varade, C. Achim, R. Naaman, *Adv. Mater.* **2018**, *30*, 1706423.